2014

A Mathematical Model of Collagen Lattice Contraction

J. C. Dallon
Brigham Young University, dallon@math.byu.edu

Emily J. Evans
Brigham Young University

H Paul Erhlich
Hershey Medical Center

Original Publication Citation

Journal of the Royal Society Interface 11:20140598 (2014)doi: 10.1098/rsif.2014.0598

A Mathematical Model of Collagen Lattice Contraction

J. C. Dallon*
Department of Mathematics,
Brigham Young University,
Provo, UT 84602-6539

E. J. Evans
Department of Mathematics,
Brigham Young University,
Provo, UT 84602-6539

H. Paul Ehrlich
Division of Plastic Surgery,
Hershey Medical Center, Hershey, PA

September 22, 2014

Abstract

Two mathematical models for fibroblast-collagen interaction are proposed which reproduce qualitative features of fibroblast populated collagen lattice contraction. Both models are force based and model the cells as individual entities with discrete attachment sites; however, the collagen lattice is modeled differently in each model. In the collagen lattice model, the lattice is more interconnected and formed by triangulating nodes to form the fibrous structure. In the collagen fiber model, the nodes are not triangulated, are less interconnected, and the collagen fibers are modeled as a string of nodes. Both models suggest that the overall increase in stress of the lattice as it contracts is not the cause of the reduced rate of contraction, but that the reduced rate of contraction is due to inactivation of the fibroblasts.

1 Introduction

In 1972 Elsdale and Bard first reported the contraction of collagen gels by fibroblasts [1]. Seven years later, Bell and coworkers introduced the fibroblast populated collagen lattice (FPCL) contraction model [2] with the goal of better understanding how contraction affects closure of an open wound. The FPCL system is intended to mimic cell matrix interactions which occur in wound granulation tissue. Although much has been learned from this system, there are still many fundamental open questions. In this paper we develop two-dimensional mathematical models designed to investigate the role of cellular forces in contracting lattices.

We describe two mathematical models which predict FPCL contraction for lattices with various cell densities. In Section 2 we give necessary background including a description of free-floating and constrained lattices, a brief discussion of myofibroblasts and fibroblasts, and a review of some previous modeling efforts. In Section 3 we present a description of the experimental methods and the numerical software used in the implementation of our model. Section 4 describes two separate mathematical models - one with a collagen lattice structure and one with a collagen string structure. In Section 5 we describe the results of our numerical simulations and we conclude with a discussion in Section 6.

2 Background

Since their introduction, several modifications have been made to FPCLs to model different biologically relevant lattices. The two most frequently studied lattices are free-floating lattices and constrained lattices. Free-floating

*To whom correspondence should be addressed. E-mail dallon@math.byu.edu

lattices float on the medium and are allowed to freely deform. Although there are local stresses in these lattices, they are imposed by the collagen structure within the lattice [3]. The constrained lattices have external forces imposed on the lattice which constrain the shape of the lattice. In this manuscript we will restrict our study to free-floating lattices. For a more complete review of FPCLs the reader is referred to [4].

Fibroblasts in FPCLs exhibit two phenotypes, the normal phenotype (referred to as fibroblast) and the myofibroblast phenotype. The myofibroblast phenotype is characterized by the expression of α-SMA, the presence of bundles of contractile microfilaments, and extensive cell-to-matrix attachments. Myofibroblasts appear to exert greater forces than fibroblasts, are more adhesive to the extracellular matrix and therefore less motile, and produce more extracellular matrix proteins [5, 6, 7]. The predominant phenotype in a lattice is dependent on experimental design [8].

There are several mathematical models of cell-extracellular matrix interactions which focus on the forces involved. Early models treated the cells and the extracellular matrix as continuum variables and used classical mechanical laws for continuum media to formulate the partial differential equations used in the models [3, 9, 10, 11, 12]. Later, in an effort to better model the collagen network, Baracos and coworkers [13, 14, 15] developed a hybrid method which considers the fibrous structure to determine forces in a volume averaging way and thus deduce the biomechanical properties of collagen tissue. On one scale they consider the extracellular matrix as a discrete fibrous structure, but in solving the tissue properties they use a continuum description. Our models, however, do not use a continuum description of the extracellular matrix or the cells.

There are multiple discrete models that are relevant to the model presented in this manuscript. Stein and colleagues [16, 17] model three dimensional collagen structures with discrete fibers. They consider these fibers as stiff rods which can twist at cross linking points to determine the deformation of the lattice. Schluter and coworkers [18] takes a more phenomenological approach to model a single cell and discrete fiber interactions to understand how the extracellular matrix affects the migration of cells. In their model, they model a drag force on the cells through the matrix and realign the matrix in the direction the cell is moving. Reinhardt and coworkers [19] use an agent-based model to simulate both complex extracellular matrix remodeling and durotaxis. They model the force interactions between discrete fibers and cells using the Fruchterman-Reingold algorithm [20] where the links between the cell and the binding site act as springs and the binding sites act as electrically charged particles. This model has the advantage of straightening collagen fibers, however in this paper they only consider one or two cells. Finally, there are modeling efforts which use a discrete fiber formulation to derive a closed form for the strain energy [21]. The goals of this last type of work are quite different from ours.

The model presented in this paper is a discrete force-based model that models the interaction between fibroblasts and a collagen lattice. This model differs from the previously described models as we model an entire lattice with many cells and focus on the contraction of the entire lattice. This model also differs from perviously described models as we allow for compaction (a biochemical process) and also for differing cell types (fibroblasts and myofibroblasts).

3 Methods

3.1 Cell lines

Human dermal fibroblast cultures were derived from neonatal foreskin explants and maintained in complete DMEM, Dulbecco's modification of Eagles medium, with 10% fetal bovine serum and 15 micrograms/ml of gentamicin. Fibroblasts were studied between their 8th and 12th passage. Dulbecco's modification of Eagle's medium (DMEM) and FBS were purchased from Life Technologies (Rockville, MD).

3.2 Casting Populated Collagen Lattices

Fibroblast PCL containing either 3,000, 10,000, 30,000, or 100,000 cells per ml of 1.25 mg of acid soluble rat tail tendon collagen in 1 mM HCl and complete DMEM. In a 60 mm Petri dish 0.2 ml drops of cell-collagen-medium mix were pipetted onto the surface of Petri dishes and allowed to polymerize before adding 2 ml of complete DMEM, which freed the lattices from the dish. Between 4 and 5 PCLs in each dish were maintained at 37°, with

5% CO_2 in a water saturated atmosphere incubator for 3 days without a change of medium. The diameter of the cell populated collagen lattices was measured initially and every 5 hours until 40 hours had elapsed.

3.3 Numerical methods

The numerical computations for our models utilize the following software packages. Initial triangulations for the collagen lattice model are created with Triangle [22]. The system of differential equations used to model the system is solved using SUNDIALS CVODE [23]. To determine the contraction of our simulated collagen we compare the area of the original lattice with the area of the contracted lattice. These areas are determined by taking the area of the convex hull of the node locations determined by qhull [24]. In order to find model parameters which would give results fitting the data, we used the optimization software gsl [25]. Finally we used MATLAB to visualize our results.

4 Model

Our mathematical model is force based and models both the cells and the collagen lattice. Although there is a significant amount of biochemical remodeling of the extracellular matrix by fibroblasts in both the wound environment and in collagen lattices, in the first 24 to 48 hours after casting a FPCL there is not much collagen deposition by the fibroblasts. The contraction of the FPCL therefore seems to be due to the forces generated by the fibroblasts.

Although the model is force based, we allow the collagen fibers to compact. The compaction of collagen is the combining of fibrils into longer and thicker collagen fibril. When the distance between two collagen fibrils is small enough the fibrils will combine into a larger collagen fiber. Eventually this merging process forms longer and thicker collagen fibers. Evidence suggests this is the fundamental process which underlies wound contraction [26].

4.1 Cells

In our model we consider a collagen lattice with N cells. A single cell is modeled as K integrin based adhesion sites (I-sites) which exert force on a common location which can be thought of as the the center of mass (see Figure 1). We note that for the simulations shown in this manuscript we fix the value of K at 10. The I-sites

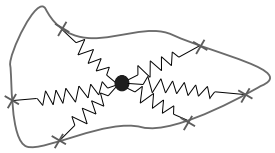

Figure 1: This figure illustrates the general ideas of how the cell is modeled mathematically. We consider a cell as a center of mass with attached springs. The other end of the springs are attached to I-sites which can interact with the extracellular matrix (membrane bound integrin based adhesion sites). In the simulations for this paper there are 10 I-sites per cell.

exert forces on the center of mass according to Hooke's law, i.e., the force is proportional to the distance from the center of mass. We may think of this as if the I-sites are attached to the center of mass with springs which have rest length ℓ, set to be zero except in simulations with the stress dependent contraction mechanism and the stress dependent mechanism (see Section 5.1). The drag on the center of mass is modeled as a sphere in water with low Reynolds number and is proportional to its velocity. The equation of motion for the center of mass of the ith cell is given by

$$C\mathbf{x}_i' = -\sum_{j=1}^{K} \alpha(||\mathbf{x}_i - \mathbf{y}_{p_{i,j}}|| - \ell)\frac{\mathbf{x}_i - \mathbf{y}_{p_{i,j}}}{||\mathbf{x}_i - \mathbf{y}_{p_{i,j}}||}, \tag{1}$$

where $\mathbf{x}_i$ is the location in $\mathbb{R}^2$ of the cell center, and $\mathbf{x}_i'$ represents the velocity of the cell and $i = 1, \cdots, N$. The spring constant which defines the cell force is α, the rest length of the spring is ℓ, and the drag coefficient is C. The right hand side of the equation expresses the forces present on the cell center from the integrin attachments, and the left side of the equation expresses the motion of the cell. If the I-sites remained permanently attached, the cell would eventually reach an equilibrium position and both sides of the equation would equal zero. The Reynolds number is low, thus because of the relative magnitudes of the coefficients, the acceleration term on the right hand side of the equation is set to zero.

We constrain the location of the I-sites to be at lattice nodes which are specific locations on the lattice (see Sections 4.2 and 4.3). The lattice node locations are denoted by $\mathbf{y}_k$, and I-sites from the same cell or other cells can be attached to the same node location. The set of indices $p_{i,1}, p_{i,2}, \cdots, p_{i,K}$ specify the lattice nodes are associated with the I-sites of cell i.

The I-sites remain attached to a node for a random amount of time, taken from a Poisson distribution with mean 60 seconds (for simulations with the stress dependent attachment mechanism and the stress dependent mechanism the time is extended, see Section 5.1). Once an I-site detaches, it immediately reattaches, thus, there are always K attachment sites for each cell. To determine the new attachment node we determine a direction and a distance from the cell center. The direction is chosen by choosing a value from a uniform distribution over the interval $[-2, 2]$ and then perturbing the angle of direction for the previous location of the I-site by this value. Once the direction is fixed, the distance is chosen from a uniform distribution between 0 to 115.726 microns, from the cell center. Once the direction and angle have been determined we negate the distance with probability 0.2. This has the affect of reversing the direction the I-site reaches in 20% of the cases. Finally we allow the I-site to attach to the nearest lattice node. For more information about the I-sites the reader is referred to a related model discussed in [27].

4.2 Collagen lattice

The collagen lattice is modeled by several nodes which are connected to form a network of spring-like connections (see Figure 2). To create the collagen lattice, M nodes are placed in the domain and the connections between

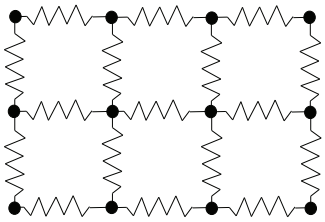

Figure 2: This figure depicts the way the collagen lattice is modeled mathematically. The collagen lattice is defined by nodes which are connected by spring-like elements. Although the nodes are regularly spaced in the figure, in most simulations they are randomly placed.

the nodes are determined through the use of a Delaunay triangulation [28]. Recall the cell I-sites are constrained to be at lattice nodes, as shown in Figure 3.

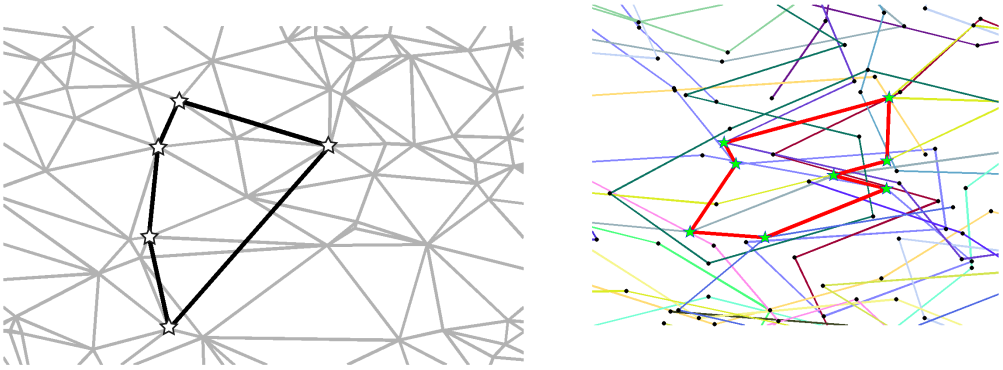

Figure 3: This left panel depicts a model cell interacting with the collagen lattice and the right panel depicts one interacting with collagen strings. The lattice is depicted by grey lines and the "cell membrane" (the convex hull of the I-sites) is shown with black lines. The stars indicate I-sites. In the left panel the I-sites (stars) are all located at the intersection of grey lines, in the right panel there are identifiable strings in the matrix and the I-sites are not constrained to be at intersection of strings.

Forces acting on lattice nodes come from the lattice or the cells. The equation of motion for the lattice node k is

$$\gamma \mathbf{y}_k'(t) = \overbrace{\sum_{m=1, m\neq k}^{M} \mathbf{f}_{k,m}(t)}^{\text{force due to lattice entanglement}} + \overbrace{\sum_{i=1}^{N} \mathbf{c}_{i,k}(t)}^{\text{force due to cells}}. \tag{2}$$

The first summation on the right hand side denotes the forces due to connections to other lattice nodes. Only the nodes directly connected to node k can have non-zero forces. The second summation on the right hand side gives the forces due to cells which have I-sites bound to node k (see Figure 3).

Lattice forces come from connections with other nodes and are classified into two types: normal or compacted. Having the second type of connection allows the compaction of collagen and is a non-reversible process. The forces due to both types of connections are spring-like in that if the connection is stretched the force is proportional to the stretching. If a normal connection is compressed however, there is no force generated. This assumption is due to the nature of collagen. When the collagen fibrils are pulled they resist the pulling due to their association with other fibrils. Yet if a cell exerts forces at two points along the same fibril drawing the two points closer, the fibril is not compressed but becomes slack between the two points similar to a rope. Compacted links act as true springs, in that, when a link is compressed a force is exerted. Thus the force due to a lattice connection between node k and node m is defined as:

$$\mathbf{f}_{k,m}(t) = \begin{cases} 0 & \mathbf{y}_k \text{ and } \mathbf{y}_m \text{ are not linked,} \\ 0 & d_{k,m} < \ell_{k,m} \text{ and the link is normal,} \\ -\beta(d_{k,m} - \ell_{k,m})(\mathbf{y}_k - \mathbf{y}_m)/d_{k,m} & \ell_{k,m} \leq d_{k,m} \text{ and the link is normal,} \\ -\beta^*(d_{k,m} - \ell^*_{k,m})(\mathbf{y}_k - \mathbf{y}_m)/d_{k,m} & \text{if the link is compacted.} \end{cases} \tag{3}$$

Here $\mathbf{y}_m$ is the location of lattice node m, $d_{k,m} = ||\mathbf{y}_k - \mathbf{y}_m||$ is the distance between node k and node m, $\ell_{k,m}$ is the rest length of the connection between node k and node m and is set as the initial distance between the nodes at the beginning of the simulation, β is the spring constant for normal links, $\beta^* = d_\beta \beta$ is the spring constant for compacted links, and $\ell^*_{k,m} = d_\ell \ell_{k,m}$ is the rest length for the spring connecting node k with node m when the link is compacted. Initially all links are normal and become compacted if the distance between two linked nodes becomes small enough, that is, if $d_{k,m} < d_p \ell_{k,m}$. When links are compacted the rest length of the spring is shortened ($d_\ell < 1$), the spring constant is increased ($d_\beta > 1$), and the link resists compression.

The forces due to the cell i are defined by:

$$\mathbf{c}_{i,k}(t) = \sum_{j=1}^{K} \alpha(||\mathbf{x}_i - \mathbf{y}_{p_{i,j}}|| - \ell) \frac{\mathbf{x}_i - \mathbf{y}_{p_{i,j}}}{||\mathbf{x}_i - \mathbf{y}_{p_{i,j}}||} \delta(p_{i,j} - k), \tag{4}$$

where $\mathbf{x_i}$ is the cell center location, $\mathbf{y_{P_{i,j}}}$ is a lattice node location, α is the spring constant and ℓ is the rest length of the integrin. Here $\delta(0) = 1$ and $\delta(x) = 0$ for any non-zero x and indicates whether the jth I-site of cell i is interacting with node k.

4.3 Collagen Strings

We now introduce an alternate model formulation for the collagen lattice. Rather than place M nodes arbitrarily in a domain in $\mathbb{R}^2$, and then interconnect them using the Triangle program we instead create collagen strings. These strings can be thought of as a chain of collagen nodes which are connected by normal connections, that is, the connections behave as springs when stretched but do not resist compression (see description of normal connections in Section 4.2).

To create a collagen string lattice, we first fix a distance between the nodes of 100 microns and set a string length by specifying the number of lattice nodes in the string. We have the option of arranging the strings in an orderly fashion to mimic spun collagen [29], however to better compare this model to the lattice model we instead allow them to arrange in a random fashion. We do this by randomly selecting a starting position in our domain and selecting the angle formed between two segments of our string from a uniform distribution in the interval $[\pi/6, 11\pi/6]$ to avoid kinks. We continue this process until a string of the desired length is created. We repeat the process for each collagen string until the desired density of collagen nodes is reached.

We now note a fundamental difference between the collagen string model and the collagen lattice model. In the lattice model, all node linking is done before any simulations are run. In the collagen string model, nodes are allowed to link at each time step if they are within 5 microns of each other. When nodes are linked in this scenario they form a compacted connection.

4.4 Model Parameters

Our model contains many parameters but the most important parameters for accurately modeling collagen lattice contractions are:

- α which represents the force the cells exert on the lattice,
- β which is Young's modulus for normal collagen and,
- β^* which is Young's modulus for compacted collagen.

These parameters have a large range of values reported in the literature.

The force that fibroblasts exert on the extracellular matrix (i.e., the value of α) is measured using four different techniques [7]. Each technique gives very different values which results in a wide range of reported fibroblast forces in the literature from 1nN to 2.65μN. The first technique is to measure the deformation of a silicon substrate by fibroblasts [30, 31]. This technique gives the highest force measurements. The second method is to measure the deformation of micro-machined devices by fibroblasts [32, 33]. The third technique measures forces on FPCLs and determines the average force exerted by a single fibroblast [34, 35]. The previous two techniques report forces in the range of 0.1 nN to 138 nN. The fourth technique uses column buckling theory to determine the force of individual fibroblasts in fabricated lattices [36]. They find that fibroblast exert average forces ranging from 11-41 nN with an upper limit of 450 nN. With such a wide range of values reported in the literature we choose to optimize the parameter α with others to try to best fit the experimental data.

Young's modulus for collagen gels (which depend on the makeup of the gel and whether the modulus is compressive or tensile) ranges from .004-24 kPa [3, 37, 38, 39, 40, 41]. Like the spring constant for the cells, this parameter will be optimized in order to fit experimental data.

We chose a value of 60 seconds for the average duration of the I-site attachments arbitrarily. The only data for this parameter which we are aware of is for Dictyostelium cells and cervical cancer cells [42, 43]. We ran simulations with values varying from 6 minutes to 10 seconds for the average duration of the I-sites. Although the contraction graphs varied, the qualitative conclusions remain valid for all values used.

5 Results

The first goal of our work is the determination of appropriate numerical parameters for α, β and β^* so that the numerical simulations will match the experimental observations. Our experimental method is detailed in Section 3 and the results for lattices with 3,750, 10,000, 30,000, and 100,000 cells per ml, gathered over a period of 40 hours, are shown in Figure 4. For the numerical simulations, we assumed that only fibroblasts exist in the collagen lattice. We ran our numerical simulations for contraction with both collagen lattices and collagen strings with four different cell densities matching those in the experimental data.

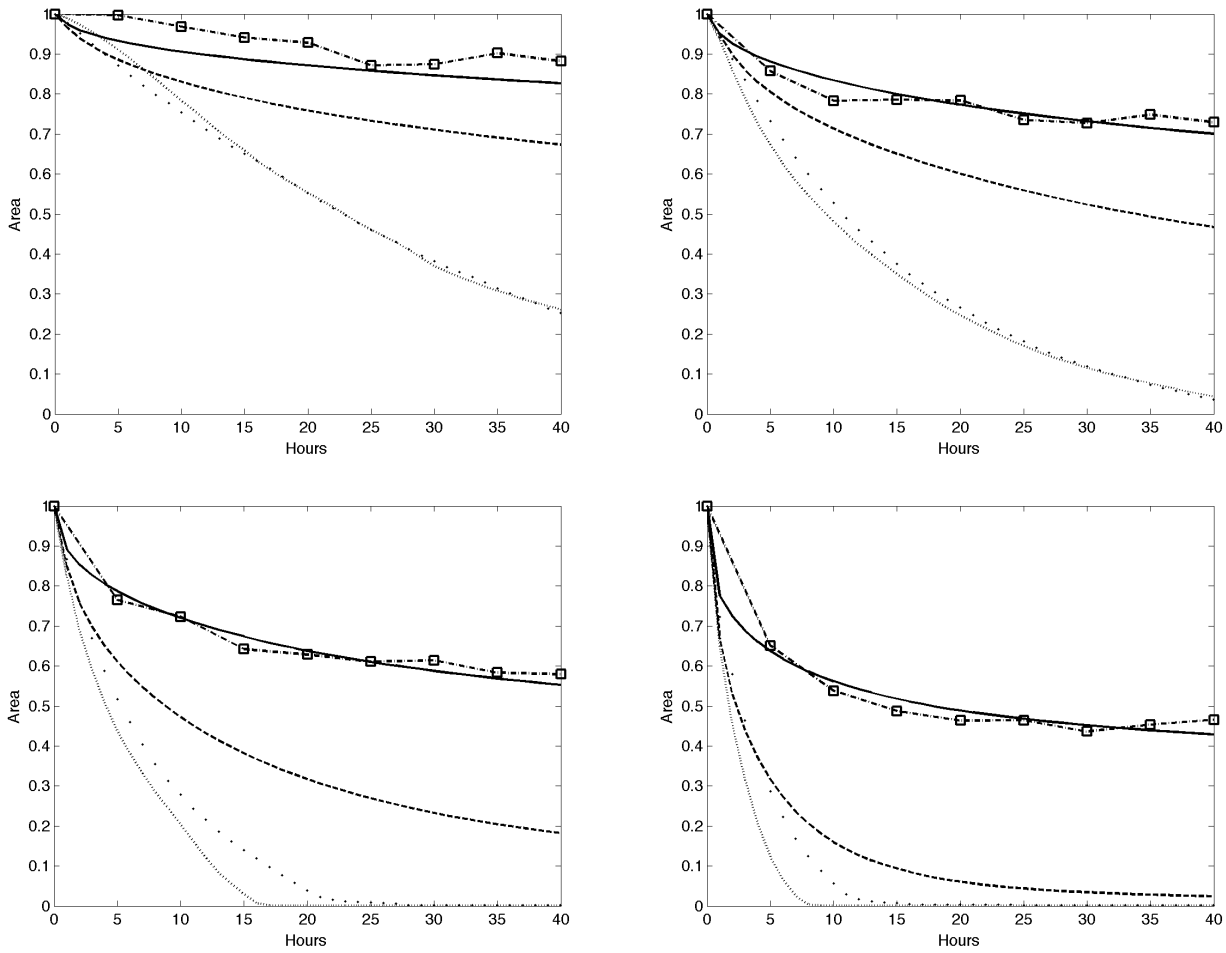

Figure 4: The lattice contraction of four different collagen lattice simulations are compared to the experimental data. In the top left panel the cell density is 3750 cells per ml, in the top right 10,000 cell per ml, in the bottom left 30,000 cells per ml and in the bottom right 100,000 cell per ml. The squares indicate the experimental values, the solid line indicates the simulations with stress dependent mechanism - stress dependent l-sites and cell contraction (incorporating both the stress dependent attachment mechanism and stress dependent contraction mechanism), the dashed line indicates simulations with the stress dependent attachment mechanism (with l-sites which become permanent with high forces), the dots indicate the simulations with the stress dependent contraction mechanism - stress dependent cell contraction (stronger cells which resist compression), and the dotted line indicates simulations with standard cells. The parameter values for the simulations are $\frac{C}{\beta} = 0.193$ hours, $\frac{\alpha}{\beta} = 2.239$, $\frac{\gamma}{\beta} = 0.114$ hours, $d_\beta = 250.538$, $d_\ell = 0.365$, $d_p = 0.365$, $A_f = 0.172$, and $A_l = 59.954$ microns.

5.1 Collagen Lattice Results

Scaling the equations by $\frac{1}{\beta}$ and using least squares to determine the best fit we varied the following values to find the best fit to the experimental observations: $\frac{C}{\beta}$, C is the cell drag coefficient; $\frac{\gamma}{\beta}$, γ is the collagen drag coefficient; d_ℓ the factor by which the collagen rest length is decreased when it is compacted; d_p the factor which determines when the links compact; $\frac{\alpha}{\beta}$, α is the spring constant determining the force the cell exerts on the collagen; and d_β the factor which increases the spring constant of the collagen when it is compacted. Although we were able to find parameter values that gave a good fit to any single cell density, we were unable to find parameter values that were valid for more than one cell density. We refer to these simulations as standard simulations.

This inability to find a set of parameters valid for all the cell densities motivated a closer study of the experimental results. In these results there are two main features: an initial fast decrease in size of the lattices and then a leveling off as the lattice size stabilizes and decreases less quickly. The main difficulty with our initial optimization was matching both these behaviors. In order to match both features we altered the model to allow the cells to have stress dependent I-sites and contraction.

We modified our model to simulate three other cases. The first modification allowed the attach time of an I-site to depend on the force applied to the I-site and is referred to as the stress depended attachment mechanism. Although this is not experimentally verified, due to the mechano-sensing ability of cells it is a reasonable assumption. For simplicity, we set the attach time to be longer than the simulations effectively making the I-site permanently attached. To implement this modification we introduce two new parameters to the model. The first, A_l, is the minimum length the integrin must be stretched, and the second A_f is a force factor. Both components are necessary since the forces on a lattice node depend on the lattice forces due to entanglement and the force due to the cells. For example, if the I-site is attached to a highly entangled region of the lattice and the I-site is far from the cell center the net force on the lattice node may be low, yet if the I-site is close to the cell center and the lattice not entangled the net force would still be low. Thus a low net force for a distant I-site indicates a region of high entanglement in the lattice but a low net force for a close I-site may not indicate a region of high lattice entanglement. The precise rule for the stress dependent attachment mechanism is: if the net force on the node (as determined by its velocity) is less than $A_f A_l \alpha$ and $||\mathbf{x}_i - \mathbf{y}_{p_{i,j}}|| > A_l$ where i denotes the cell and j denotes the I-site, then the I-site becomes permanently attached. Implementing this rule and optimizing on the parameters A_f and A_l in addition to the original parameters still did not give the desired results. Cells with the stress dependent attachment mechanism did not simulate the data any better than the standard simulations.

In the next set of simulations we implemented a stress dependent cell contraction mechanism. This modification was made by allowing the allowing the cells to become stronger when the same threshold as the stress dependent attachment mechanism to fix the I-sites was reached. In simulations with the stress dependent cell contraction mechanism the I-sites were not fixed but the cell's contraction properties changed so that they exerted greater forces and resisted compression. This was done by multiplying the force the cells exert, α, by 10 and by changing the rest length of the I-site adhesion to be its length at the first time the rule indicated stronger forces. The simulations with cells having the stress dependent cell contraction mechanism did not give satisfactory results. Simulations which did not fix the length of the l-sites to be the new length but had the greater force also failed.

Our final simulation combined the stress dependent attachment mechanism and the stress dependent cell contraction mechanism to create the stress dependent mechanism. Optimizing the parameters where cells had both the stress dependent attachment mechanism and the stress dependent contraction mechanism gave results which matched the data (see Figure 4 solid lines). The figure also shows the effect of removing either or both of the new cell mechanisms. The simulations in Figure 4 use the same parameter set which was optimized for the stress dependent mechanism simulations. These results suggest that allowing cells to resist compression and have permanently attached I-sites is important in matching the rate of cell contraction in the free floating lattices.

Having found simulations which matched the data, we examined the cell distribution at the conclusion of the simulations using the stress dependent mechanism. Figure 5 shows the initial cell distribution in the left panels for each cell density and the final cell distribution in the right panels for each cell density. Figure 6 shows the results from a simulation with 500,000 cells per ml. After 40 hours the cells are much more concentrated near the boundary of the lattice with the cell density in the interior of the lattice being about 84,000 cells per cm squared

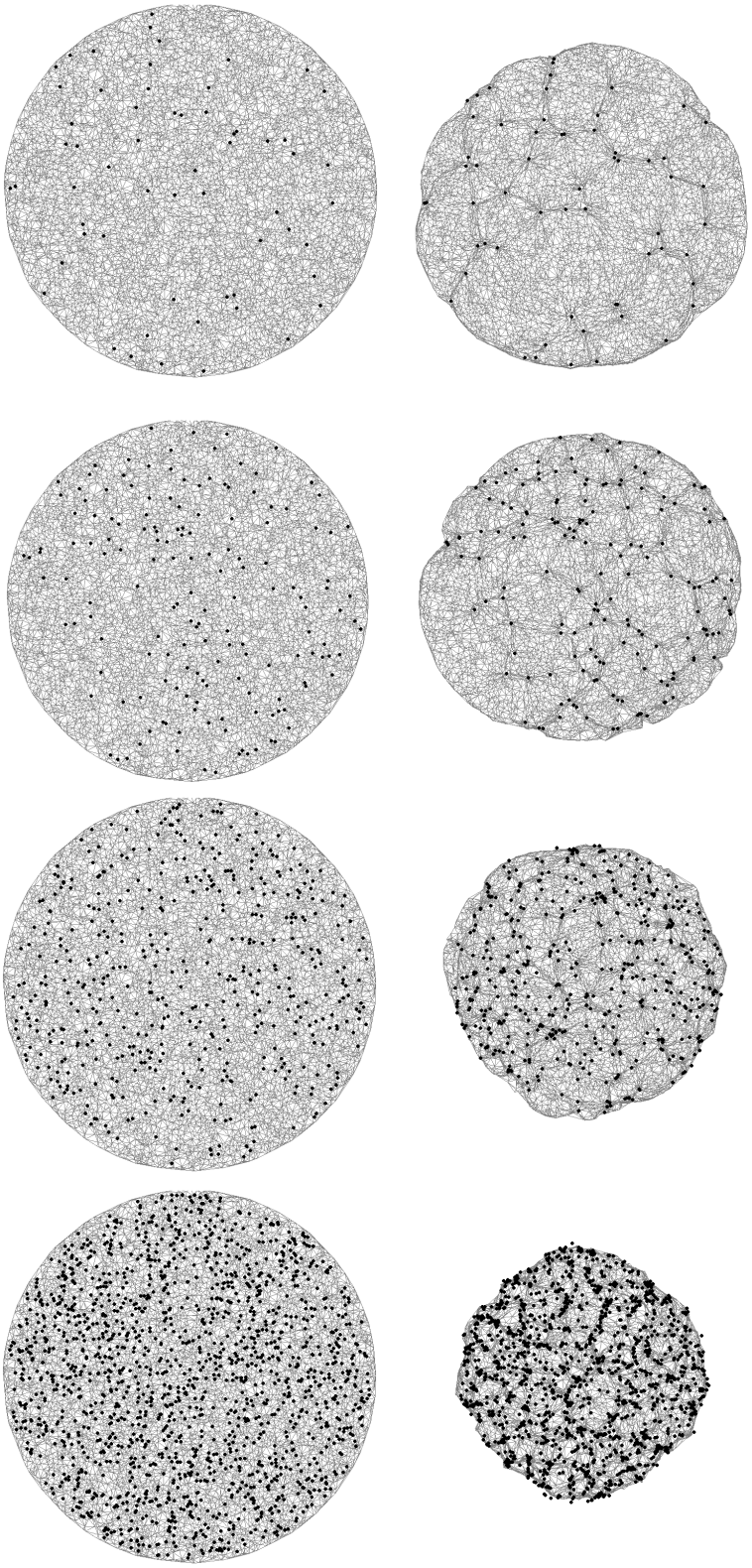

Figure 5: The initial and final configuration of the lattices are shown for four different densities with the cell center marked as solid circles. The top row is the 3750 cells per ml, the second row 10,000 cells per ml, the third row is 30,000 cells per ml, and the fourth row is 100,000 cells per ml. The right panels show the initial configuration and the left panels show the configuration after 40 hours. The simulations shown here correspond to the simulations for the solid lines in figure 4.

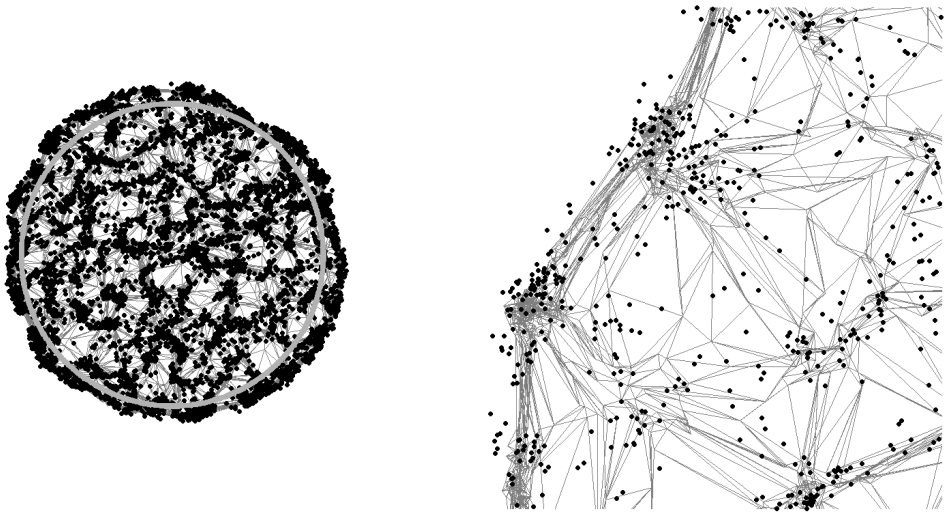

Figure 6: The cell density for a simulation with 500,000 cells per ml is shown after 40 hours. In the left panel the light gray circle shows the boundary for the region where the interior density is calculated. The edge density is calculated using the convex hull of the lattice minus the circular region used for the interior density. The right panel shows the edge of the lattice magnified. Observe the highly organized collagen structure at the lattice edge. Other than the cell density the parameters are the same as the simulation shown in Figure 5. The cells centers outside of the lattice are due to the fixed spring size of the I-sites in simulations with the stress dependent mechanism.

and the cell density at the edge being about 250,000 cells per cm squared. The lattice is also compacted in a tight ring around the edge. Both of these features are seen experimentally [3, 44]. The experiments by Ehrlich et. al. use a cell density of 500,000 cells per ml and the experiments in Simons et. al. have a cell density of 50,000 cells per ml. To determine if the same trend held for the simulations with 100,000 cells per ml we averaged the interior cell density and the boundary cell density for 102 runs with the same initial lattice configuration but different random initial positions for the cells and different instantiations for the random behavior of the cell motion. The results confirm the same characteristic of the final cell distribution. The average cell density at the boundary of the lattice at 40 hours was 31,423 cells per cm squared and the average cell density for the interior was 20,074 cells per cm squared. Figure 7 is a magnification of the edge of the lattice shown in Figure 5 bottom right panel. Again a dense ring of collagen can be seen at the edge, just not as prominent as in the higher density case.

We also examined the amount of force each cell was exerting at the final time of the simulation (40 hours) and the spatial distribution of the cells. The results are shown in Figure 8. The insets show the scatter plot of the cell forces plotted against the radius of the lattice. The average force the cells exert with respect to radius seems to remain relatively constant. This should not be confused with the stiffness of the lattice which likely varies. The contraction data indicates that the lattice is approaching an equilibrium of forces (i.e. the cell forces and the lattice forces are equilibrating and the contraction is leveling off).

5.2 Collagen String Results

Once a set of valid parameters were found for the collagen lattice we wished to simulate the same four cell densities using the collagen string model. We began by simulating the standard case with the expectation that again a poor fit would be found to the experimental data. As can be seen in Figure 9 the standard case results in excessive contraction. It is worth noting though that when the collagen string case is compared to the collagen lattice case less contraction occurs for the string case. The reason for this decrease in contraction is due to the fact that the collagen strings are less interconnected initially. As the strings are contracted compaction occurs and the strings become interconnected, however there still exist collagen nodes that are connected to only one or two other nodes. This creates "collagen fingers" which trail the contraction occurring in the model. For a visualization of these fingers see Figure 11.

Knowing that the stress dependent mechanism was critical to good experimental match for the collagen lattice model we ran simulations using the stress dependent mechanism. Our goal was to minimize the number of

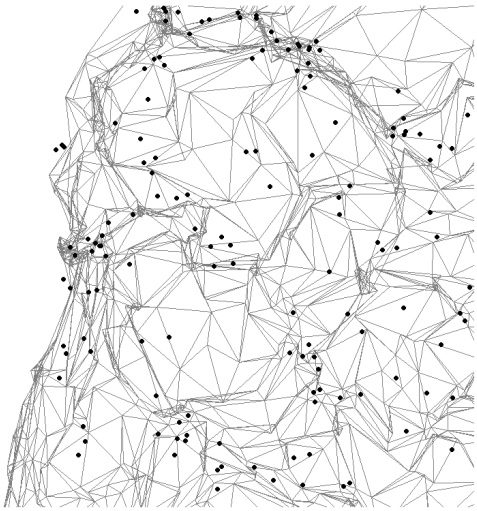

Figure 7: Magnification of the bottom right panel of Figure 5. Observe that the collagen structure near the edge is more dense than in the interior. The trend is not as prominent as the simulations with a higher cell density. The cell density for this simulation is 100,000 cells per ml and the lattice is shown after 40 hours.

parameters that must be changed in order to match the experimental data. We discovered that it was possible to closely match the experimental data by changing only the force factor A_f. Recall that the force factor was used in the stress dependent rule to change the cell behavior, that is, if the net force on the node (as determined by its velocity) is less than $A_f A_l \alpha$ and $||\mathbf{x}_i - \mathbf{y}_{p_{i,j}}|| > A_l$ where i denotes the cell and j denotes the I-site, then the I-site becomes permanently attached. The values of A_f used were 0.00286718, 0.005818, 0.026718 and 0.126718 for cell densities of 3750 cells per ml, 10,000 cell per ml, 30,000 cells per ml, and 100,000 cells per ml respectively. In order to maintain the closest possible match to the parameters used for the collagen lattice case we allowed for different values of A_f. The reason for the higher force factor for the higher concentration is that with so many cells pulling on collagen nodes a higher tension exists initially. The higher value of A_f allows for cells to contract the collagen lattice for a short time until the tension surpasses a factor of the original tension. In the lower density cases the initial tension is lower so a lower force must be used to trigger the conversion to permanent I-sites and cells which resist compression and are stronger. It is worth noting that for the collagen lattice the force factor A_f is 0.172 which is greater than any of the force factors used for the collagen strings indicating a higher initial tension. This is to be expected since the collagen lattice is more highly connected and moving one node will typically result in moving many nodes requiring a greater force. The greater connectivity of the collagen lattice distributes the cell and collagen forces over a larger region of the lattice.

We also wished to simulate cells with the stress dependent attachment mechanism and the stress dependent contraction mechanism. For simulations with the stress dependent attachment mechanism, we decreased the motility of the cells once our stress rule was met by setting the attach time longer then the simulation. This case is shown by the dashed lines in Figure 9. As shown in the figure for the collagen strings the fixing of the integrins seems to be the more important property. To run simulations with cells which have the stress dependent contraction mechanism we strengthen the cell and allowed them to resist compression (but did not permanently attach the integrin) when the stress rule was met. The results of this simulation can be seen in Figure 9. Although not as important as the fixing of the integrins, strengthening the integrins and having the cell resist compression results in significant improvements in experimental matching, especially as the density of the cells increases. Figure 10 shows the initial and final configuration of the lattices for simulations with varying cell density.

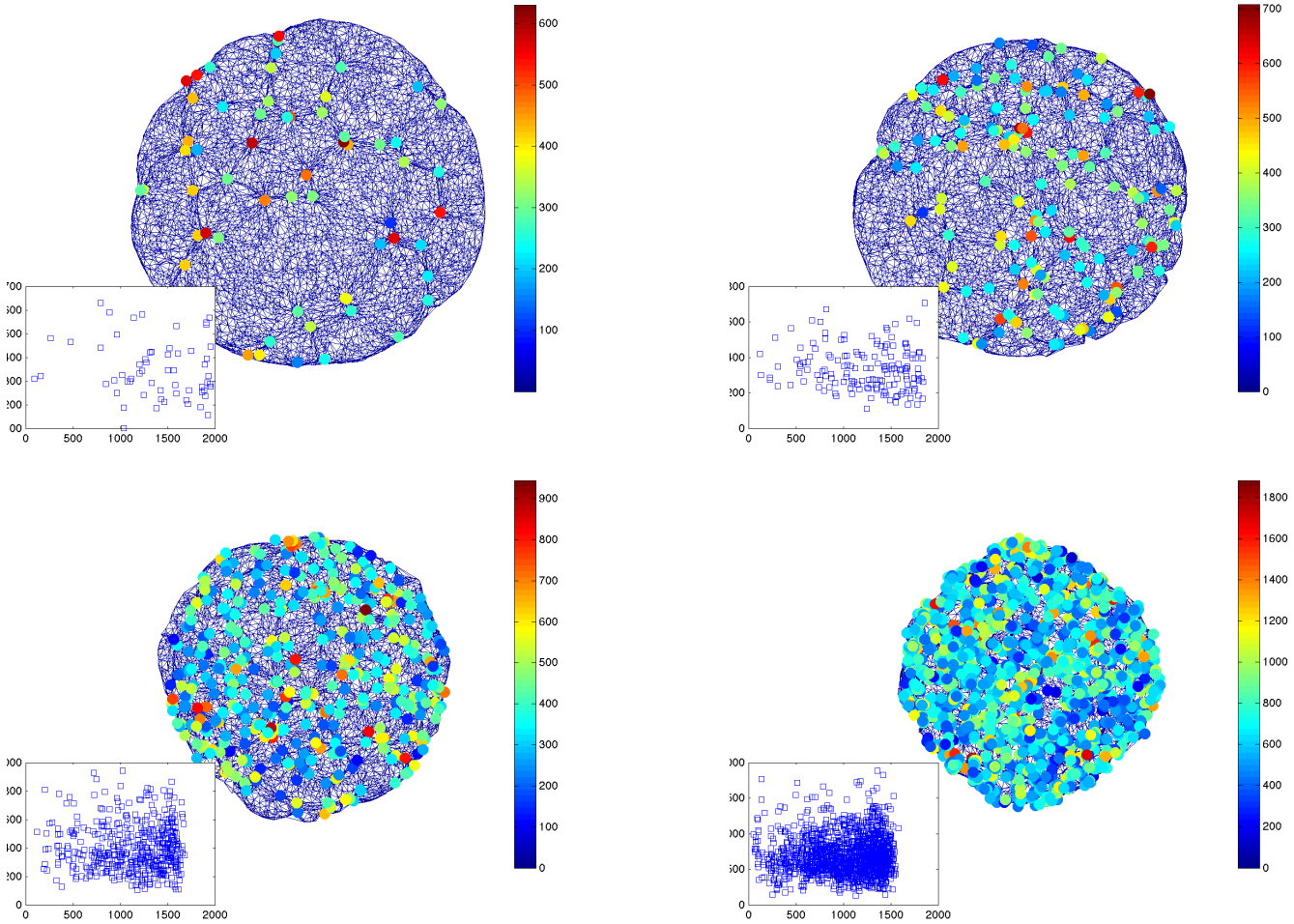

Figure 8: This figure shows the same lattices as shown in the right panels of Figure 5 with the total amount of force the cell is exerting indicated by the shading. The insets show the cell forces plotted against lattice radius. The x-axis in the inset is in microns and the force is scaled by the $1/\beta$ giving units of 1/microns. The force the cells exert do not indicate the stiffness of the lattice, only the activity of the cell.

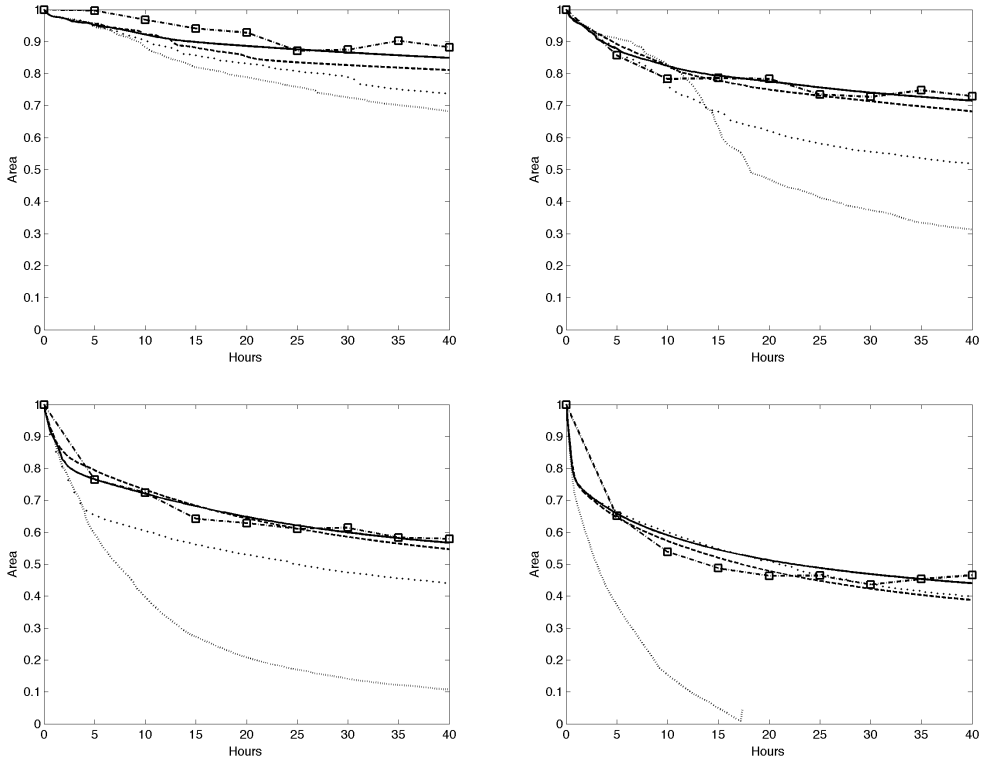

Figure 9: The contraction of four different collagen string simulations is compared to the experimental data. Everything is the same as in figure 4 except the value of A_f is varied with each simulation and had values of 0.00286718, 0.005818, 0.026718 and 0.126718 for cell densities of 3750 cells per ml, 10,000 cell per ml, 30,000 cells per ml, and 100,000 cells per ml respectively.

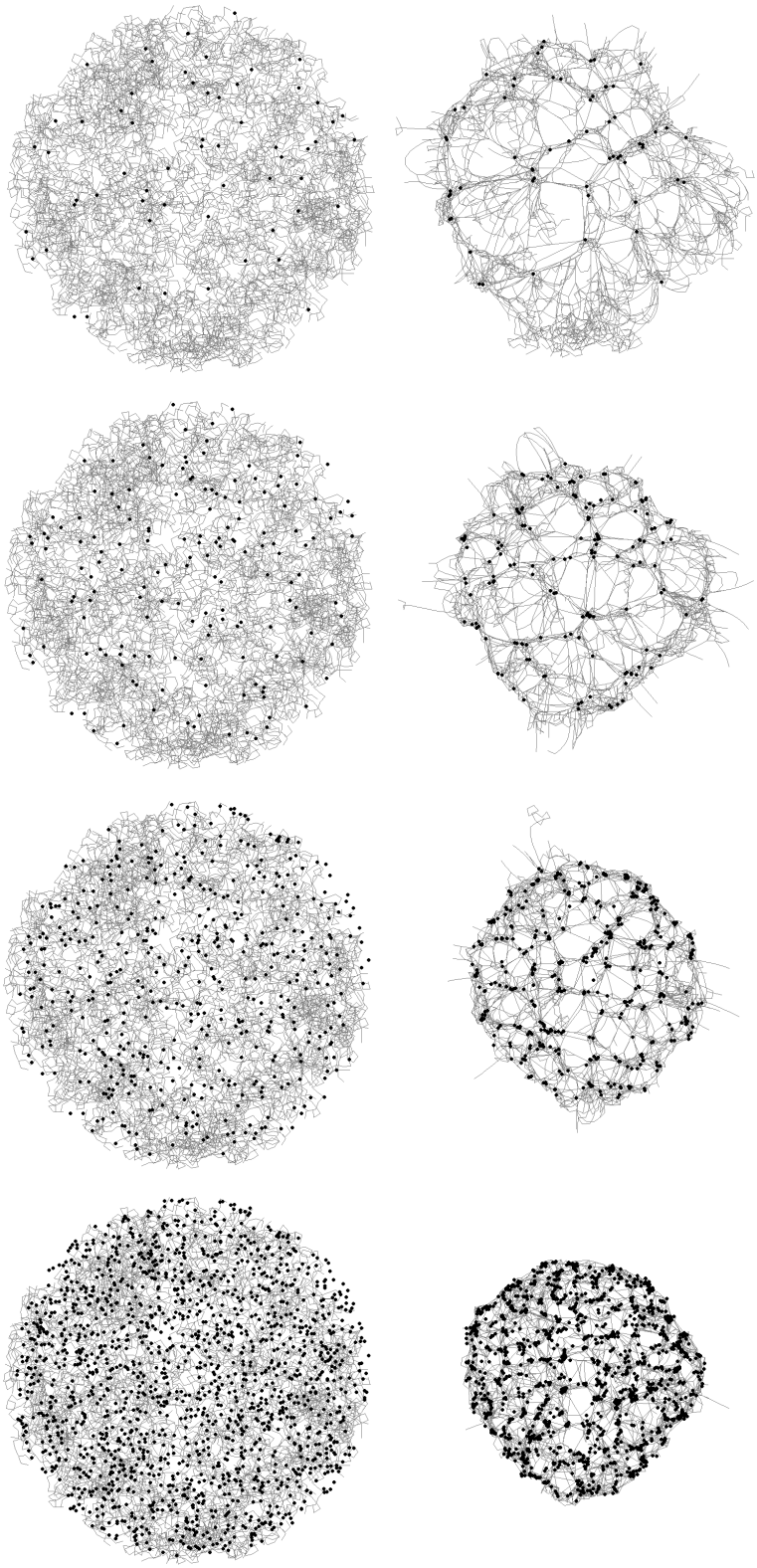

Figure 10: This figure is the same as Figure 5 except the simulations are from the collagen string model.

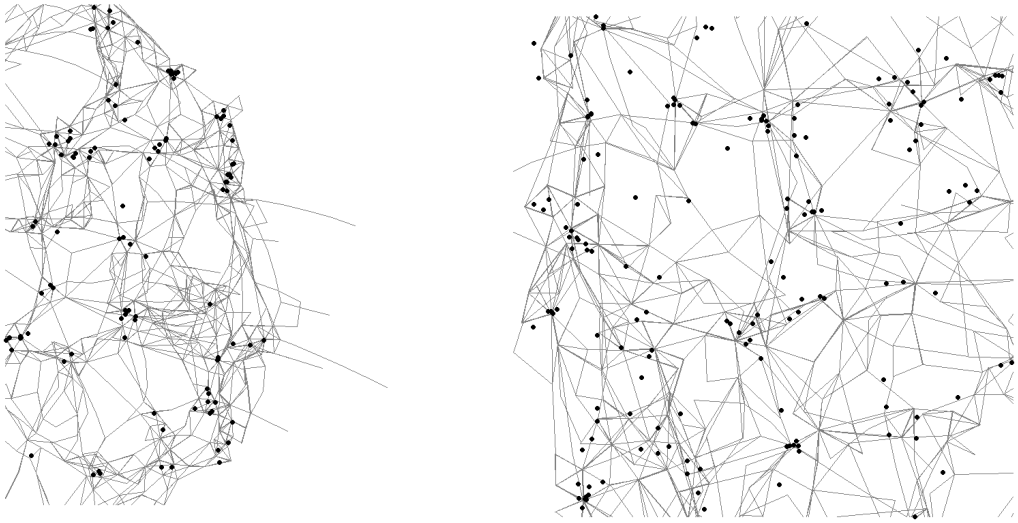

Figure 11: The left panel is a magnification of the second to bottom right panel of Figure 10. Observe the collagen fingers that extend from the collagen mass. The right panel is a magnification of the bottom right panel of Figure 10. Observe that the collagen structure near the edge is more dense than in the interior. The trend is not as prominent as for the collagen lattice simulations with a similar cell density.

6 Discussion

The mathematical models presented here offer new insights into how fibroblasts contract collagen lattices which are consistent with previous modeling work. Before performing the simulations it was unclear if the normal tension within a lattice as it contracted was sufficient to explain the experimentally observed rate of contraction. Using two different formulations for the collagen lattice this work shows that the cells have sufficient force to contract the lattices to a greater degree then what is seen experimentally. The cells must for some reason become less active during the course of lattice contraction. While we cannot prove the necessity of the transition from active cells to inactive cells, the collagen lattice model indicates that it is difficult to explain the behavior of the collagen without allowing the cells to become both immobile and stronger in resisting both stretching forces and compressional forces. Experiments show that the first 5-10 hours for all but the lowest density lattices have the greatest rate of contraction. After this initial period the lattices contract at a slower rate. The signal causing the slowing rate of contraction may be the greater local tension in the lattice. This may signal the cells to become less active in contracting the lattice, for example by becoming myofibroblasts or some other less actively contracting phenotype. These conclusions are consistent with the results of Stevenson *et. al.* [45] who proposed that a cell in the lattice contracts only the collagen local to the cell and once nearby collagen is sufficiently compacted the cell becomes dormant. Using these assumptions they were able to accurately model the cell mediated contraction of lattices (not time course data) with different collagen and cell densities. It is also consistent with the modeling results of Reinhardt *et. al.* [19] which suggest that the cells compact the matrix in the pericellular region to a greater extent than other areas. We suggest that as fibroblasts contract the lattice the local collagen structure becomes more dense and less easily deformed. The cells in essences are in a stiffer less compliant part of the matrix (which they formed) and begin to become less mobile. The new behavior of the cells results in a slowing of the rate of contraction of the entire lattice. Since the myofibroblasts phenotype is more adhesive, less motile, and stronger than the normal fibroblast phenotype, one way to test this theory would be to collect time dependent data for the contraction of free floating lattices where the fibroblasts-myofibroblast transition is promoted (perhaps by adding TGFβ). We hypothesize that a free floating lattice populated predominantly by myofibroblasts would have a slower rate of contraction.

It is interesting to note the different results in the two model formulations. The collagen lattice model gives an initial lattice which is more highly interconnected than the initial state of the collagen in the collagen string model. In the two higher density cases, the collagen string model shows that the rate of contraction slows down dramatically before 5 hours. It is this change in rate which allows the good fit to the data. By either fixing the I-sites or giving them a non-zero rest length the contraction of the lattice slows down dramatically. The same

dramatic changes is not seen in the collagen lattice simulations. Of course the forces are distributed over a larger regions in the collagen which should smooth out the transition.

The collagen lattice model not only matches the time course of free floating FPCL's for several densities but also show density features observed in experimental lattices. The mathematical simulations with higher cell densities show that the final cell density is higher near the lattice boundary and the collagen is highly organized in a ring surrounding the lattice. It appears that the free boundary is more readily contracted. An explanation for this is that the cells in the center are anchored by the surrounding cells and the surrounding collagen. In the center, cells are pulling on collagen nodes in each direction, but these collagen nodes are being pulled by other cells or other collagen nodes resulting in very little movement. Cells on the edges also pull on collagen nodes however those nodes on the edges are "free" from other cells and other collagen connections and contract into the cell. This results in a net movement of these cells towards the center. After a sufficient number of time steps this results in the increased density that can be seen.

This theory can be supported by the increased density seen in the center of the collagen string. Here the collagen nodes are more free since they are less interconnected. Further evidence supporting this idea is the more highly stretched collagen in the very high cell density case right after the collagen ring on the edge (see Figure 6 right panel) as compared to the same region in the lower cell density case (see Figure 7). There are enough cells at the periphery of the high density case to cause the greater stretching of the interior lattice. If the free edge is the cause, an annulus shaped lattice should show the same cell density and collagen rings on both the outer edge and the inner edge.

In summary both the collagen lattice and the collagen spring model show promise in mathematically modeling the contraction of collagen. An important characteristic of these models is the ability to change behavior of the cells to become stress dependent. These results show the potential for simple mathematical models to provide insight into biological processes where cells interact with an extracellular matrix.

References

[1] Elsdale T, Bard J. Collagen Substrata for Studies on Cell Behavior. J Cell Biol. 1972;54:626–637.

[2] Bell E, Ivarsson B, Charlotte M. Production of a tissue-like structure by contraction of collagen lattices by human fibroblasts of different proliferative potential in vitro. Proce Natl Acad Sci. 1979;76(3):1274–1278.

[3] Simon D, Horgan C, Humphrey J. Mechanical restrictions on biological responses by adherent cells within collagen gels. Journal of the mechanical behavior of biomedical materials. 2012;14:216–226.

[4] Dallon JC, Ehrlich HP. A review of fibroblast-populated collagen lattices. Wound Repair Regen. 2008;16(4):472–9.

[5] Ehrlich HP, Rajaratnam JBM. Cell locomotion forces versus cell contraction forces for collagen lattice contraction: An in vitro model of wound contraction. Tiss Cell. 1990;22:07–417.

[6] Hinz B. Formation and Function of the Myofibroblast during Tissue Repair. Journal of Investigative Dermatology. 2007;127:526–537.

[7] Li B, Wang JHC. Fibroblasts and myofibroblasts in wound healing: Force generation and measurement. Journal of tissue viability. 2011;20(4):108–120.

[8] Tomasek JJ, Haaksma CJ, Eddy RJ, Vaughan MB. Fibroblast contraction occurs on release of tension in attached collagen lattices: dependency on an organized actin cytoskeleton and serum. Anat Rec. 1992;232:359–368.

[9] Ferrenq I, Tranqui L, Vailhé B, Gumery PY, Tracqui P. Modelling biological gel contraction by cells: mechanocellular formulation and cell traction force quantification. Acta Biotheor. 1997 Nov;45(3-4):267–93.

[10] Olsen L, Maini PK, Sherratt JA, Dallon JC. Mathematical Modelling of Anisotropy in Fibrous Connective Tissue. Math Biosci. 1999;158:145–170.

[11] Barocas VH, Tranquillo RT. An anisotropic biphasic theory of tissue-equivalent mechanics: the interplay among cell traction, fibrillar network deformation , fibril alignment and cell contact guidance. AMSE J Biomech Eng. 1997 May;119:137–145.

[12] Murray JD, Oster GF. Cell traction models for generating pattern and form in morphogenesis. J Math Biol. 1984;19:265–279.

[13] Stylianopoulos T, Barocas VH. Volume-averaging theory for the study of the mechanics of collagen networks. Comput Methods Appl Mech Engrg. 2007;197:2981–2990.

[14] Sander EA, Stylianopoulos T, Tranquillo RT, Barocas VH. Image-based multiscale modeling predicts tissue-level and network-level fiber reorganization in stretched cell-compacted collagen gels. Proc Natl Acad Sci U S A. 2009 Oct;106(42):17675–80.

[15] Lai VK, Lake SP, Frey CR, Tranquillo RT, Barocas VH. Mechanical behavior of collagen-fibrin co-gels reflects transition from series to parallel interactions with increasing collagen content. J Biomech Eng. 2012 Jan;134(1):011004.

[16] Stein AM, Demuth T, Mobley D, Berens M, Sander LM. A mathematical model of glioblastoma tumor spheroid invasion in a three-dimensional in vitro experiment. Biophysical journal. 2007;92(1):356–365.

[17] Stein AM, Vader DA, Weitz DA, Sander LM. The micromechanics of three-dimensional collagen-I gels. Complexity. 2011;16(4):22–28.

[18] Schlüter DK, Ramis-Conde I, Chaplain MAJ. Computational modeling of single-cell migration: the leading role of extracellular matrix fibers. Biophys J. 2012 Sep;103(6):1141–51.

[19] Reinhardt JW, Krakauer DA, Gooch KJ. Complex Matrix Remodeling and Durotaxis Can Emerge From Simple Rules for Cell-Matrix Interaction in Agent-Based Models. Journal of biomechanical engineering. 2013;135(7):071003.

[20] Fruchterman TM, Reingold EM. Graph drawing by force-directed placement. Software: Practice and experience. 1991;21(11):1129–1164.

[21] Flynn C, Rubin M, Nielsen P. A model for the anisotropic response of fibrous soft tissues using six discrete fibre bundles. International Journal for Numerical Methods in Biomedical Engineering. 2011;27(11):1793–1811.

[22] Shewchuk JR. Triangle: Engineering a 2D quality mesh generator and Delaunay triangulator. In: Applied computational geometry towards geometric engineering. Springer; 1996. p. 203–222.

[23] Hindmarsh AC, Brown PN, Grant KE, Lee SL, Serban R, Shumaker DE, et al. SUNDIALS: Suite of nonlinear and differential/algebraic equation solvers. ACM Transactions on Mathematical Software (TOMS). 2005;31(3):363–396.

[24] Barber CB, Dobkin DP, Huhdanpaa H. The quickhull algorithm for convex hulls. ACM Transactions on Mathematical Software (TOMS). 1996;22(4):469–483.

[25] Galassi M, Davies J, Theiler J, Gough B, Jungman G, Alken P, et al. GNU Scientific Library Reference Manual. 3rd ed. Network Theory Ltd; 2010.

[26] Ehrlich HP, Hunt TK. Collagen organization critical role in wound contraction. Advances in Wound Care. 2012;1(1):3–9.

[27] Dallon JC, Scott M, Smith WV. A Force Based Model of Individual Cell Migration with Discrete Attachment Sites and Random Switching Terms. Journal of Biomechanical Engineering. 2013 June;135(7):071008–071008–10.

[28] Preparata FP, Shamos MI. Computational Geometry: An Introduction. New York: Springer-Verlag; 1985.

[29] Nain AS, Sitti M, Jacobson A, Kowalewski T, Amon C. Dry spinning based spinneret based tunable engineered parameters (step) technique for controlled and aligned deposition of polymeric nanofibers. Macromolecular rapid communications. 2009;30(16):1406–1412.

[30] Fray TR, Molloy JE, Armitage MP, Sparrow JC. Quantification of single human dermal fibroblast contraction. Tissue Eng. 1998;4(3):281–91.

[31] Wrobel LK, Fray TR, Molloy JE, Adams JJ, Armitage MP, Sparrow JC. Contractility of Single Human Dermal Myofibroblasts and Fibroblasts. Cell Motility and the Cytoskeleton. 2002;52:82–90.

[32] Tymchenko N, Wallentin J, Petronis S, Bjursten LM, Kasemo B, Gold J. A novel cell force sensor for quantification of traction during cell spreading and contact guidance. Biophysical Journal. 2007 Jul;93(1):335–345.

[33] Galbraith CG, Sheetz MP. A micromachined device provides a new bend on fibroblast traction forces. Proc Natl Acad Sci U S A. 1997 Aug;94(17):9114–8.

[34] Brown R, Prajapati R, McGrouther D, Yannas I, Eastwood M. Tensional homeostasis in dermal fibroblasts: Mechanical responses to mechanical loading in three-dimensional substrates. Journal of cellular physiology. 1998;175(3):323–332.

[35] Delvoye P, Wiliquet P, Levêque JL, Nusgens BV, Lapière CM. Measurement of mechanical forces generated by skin fibroblasts embedded in a three-dimensional collagen gel. J Invest Dermatol. 1991 Nov;97(5):898–902.

[36] Harley BA, Freyman TM, Wong MQ, Gibson LJ. A new technique for calculating individual dermal fibroblast contractile forces generated within collagen-GAG scaffolds. Biophysical journal. 2007;93(8):2911–2922.

[37] Grinnell F, Petroll WM. Cell motility and mechanics in three-dimensional collagen matrices. Annu Rev Cell Dev Biol. 2010;26:335–61.

[38] Mooney RG, Costales CA, Freeman EG, Curtin JM, Corrin AA, Lee JT, et al. Indentation micromechanics of three-dimensional fibrin/collagen biomaterial scaffolds. Journal of Materials Research. 2006 Aug;21(8):2023–2034.

[39] Marenzana M, Wilson-Jones N, Mudera V, Brown RA. The origins and regulation of tissue tension: identification of collagen tension-fixation process in vitro. Exp Cell Res. 2006 Feb;312(4):423–33.

[40] Chen BP, Li CH, Au-Yeung KL, Sze KY, Ngan AHW. A microplate compression method for elastic modulus measurement of soft and viscoelastic collagen microspheres. Annals of Biomedical Engineering. 2008 July;36(7):1254–1267.

[41] Velegol D, Lanni F. Cell traction forces on soft biomaterials. I. Microrheology of type I collagen gels. Biophysical journal. 2001;81(3):1786–1792.

[42] Saraiva N, Prole DL, Carrara G, Johnson BF, Taylor CW, Parsons M, et al. hGAAP promotes cell adhesion and migration via the stimulation of store-operated Ca2+ entry and calpain 2. The Journal of cell biology. 2013;202(4):699–713.

[43] Uchida K, Yumura S. Dynamics of novel feet of Dictyostelium cells during migration. Journal of Cell Science. 2004 Mar;117(8):1443–1455.

[44] Ehrlich HP, Rittenberg T. Defferences in the mechanism for high- versus moderate-density fibroblast-populated collagen lattice contraction. Journal of Cellular Physiology. 2000;185:432–439.

[45] Stevenson MD, Sieminski AL, McLeod CM, Byfield FJ, Barocas VH, Gooch KJ. Pericellular conditions regulate extent of cell-mediated compaction of collagen gels. Biophysical journal. 2010;99(1):19–28.